Anomalous Nernst thermoelectric generation in multilayer-laminated coiled magnetic wires

Ken-ichi Uchida[1,*], Tetsuya Kuwabara[2], Toru Tanji[2], Makoto Fujimoto[2], Ren Nagasawa[1], and Ryo Iguchi[1]

[1] Research Center for Magnetic and Spintronic Materials, National Institute for Materials Science, Tsukuba 305-0047, Japan

[2] Energy & Electronics Materials Laboratory, Sumitomo Electric Industries, Ltd., Osaka 554-0024, Japan

[*] E-mail: UCHIDA.Kenichi@nims.go.jp

ABSTRACT

Thermoelectric generation using the anomalous Nernst effect is demonstrated in multilayer-laminated coils comprising ferromagnetic metal wires stacked in the radial direction. By applying a temperature gradient to the coils in the radial direction, the thermoelectric voltage and power induced by the anomalous Nernst effect appear and increase in proportion to the number of the stacked layers. This device structure is useful for improving the thermoelectric performance and versatility of energy harvesting devices based on the anomalous Nernst effect.

The anomalous Nernst effect (ANE), a transverse magneto-thermoelectric conversion phenomenon in a magnetic material, converts a temperature gradient into a transverse electric field depending on the spontaneous magnetization of the magnetic material.[1-22)] In general, the transverse thermopower S in a magnetic material under a magnetic field consists of the contributions proportional to the magnetic field H and magnetization M:

$$S = Q_H \mu_0 H + Q_M \mu_0 M, \quad (1)$$

where $Q_{H(M)}$ is the proportionality factor of the H-dependent (M-dependent) contribution and μ_0 is the vacuum permeability. The anomalous Nernst coefficient S_{ANE}, the transverse thermopower due to ANE, comes from the second term of Eq. (1): $S_{\mathrm{ANE}} = Q_M \mu_0 M_{\mathrm{s}}$ with M_{s} being the saturation magnetization. The electric field driven by ANE is thus determined by

$$\mathbf{E}_{\mathrm{ANE}} = S_{\mathrm{ANE}}(\mathbf{m} \times \nabla T), \quad (2)$$

where $\mathbf{m}$ and ∇T are the unit vector of magnetization and the temperature gradient applied to the magnetic material, respectively. When $\mathbf{m}$ is perpendicular to ∇T, ANE works as a thermoelectric generator. The open-circuit voltage generated by ANE is proportional to the length of the magnetic material along $\mathbf{E}_{\mathrm{ANE}}$. Owing to this feature, ANE enables thermoelectric power generation in simple

sheet or block structures[19,21] and coiled wires[7,11] as well as heat-flux sensing in lateral zigzag structures,[15,19,22] which are conceptually different from module structures based on the Seebeck effect. In the ANE device based on coiled wires, the magnetic material is magnetized along the axial direction and a temperature gradient is applied along the radial direction to satisfy the symmetry of Eq. (2) (Fig. 1). In Ref. 11, the ANE-driven thermopower generation in coiled wires and the proportionality between the thermoelectric voltage and wire length were demonstrated, where a galfenol ($Fe_{0.85}Ga_{0.15}$) wire was used as a magnetic material. However, such experiments have only been conducted on single-layer coiled wires.

In this study, we demonstrate the ANE-based thermoelectric generation in multilayer-laminated coiled magnetic wires, where magnetic wires are stacked in the radial direction, i.e., in the ∇T direction. It is experimentally confirmed that the output voltage and power due to ANE increase in proportion to the number of stacked layers. This proof-of-concept demonstration contributes to improving the thermoelectric performance and versatility of ANE devices.

The magnetic material used in this study is a ferromagnetic polycrystalline Ni-based alloy with 3.1 at% Si, 2.2 at% Cr, and 2.1 at% Mn, prepared by a melting method. This Ni-based alloy is widely used as electrode materials in applications such as spark plugs for automobile engines. We selected this alloy because it has high ductility and the S_{ANE} value much larger than that of pure Ni (~0.2 μV/K).[24] We confirmed that, using a rectangular-shaped Ni-based alloy slab, S_{ANE} of this alloy is 1.4 μV/K by a method similar to that described in Ref. 23. Next, wires with a diameter of 0.13 mm were produced by drawing at room temperature, followed by heat treatment. For dense coiling, flat wires with a cross section of 0.22 × 0.06 mm were then produced by rolling at room temperature. The electrical conductivity of the Ni-based alloy is 2.4×10^6 S/m.

The multilayer-laminated coiled Ni-based alloy wires for the ANE-based thermoelectric generation were constructed as follows. As the basis of the coil, an oxygen-free Cu bobbin was used, of which the portion for winding the wires has a length of 36 mm and a diameter of 18 mm [Figs. 2(a), (b)]. To wind the flat wires neatly, the bobbin has a brim at the ends. The center of the bobbin has a hole with an inner diameter of 14 mm, through which a heater and thermocouple can be inserted. First, polyethylene terephthalate (PET) films with a thickness of ~0.02 mm were wrapped around the surface of the bobbin to avoid electrical conduction between the Cu bobbin and the Ni-based alloy wires. Next, the flat Ni-based alloy wire was laterally wound 40 times with a gap of ~0.5 mm, and varnish was applied to the gap and the surface of the wires, followed by drying and curing processes. The PET films were wrapped again for electrical insulation around the outside of the varnish-cured coil, which was defined as one layer. The above processes were repeated to construct three coils with $N = 1$, 5, and 10, where N is the number of the stacked layers [see the scanning electron microscope images in Fig. 2(c)]. The Ni-based alloy wires of each layer were electrically connected in series so

that the ANE voltage was enhanced. We coated the inner surface of the center hole of the Cu bobbin with cement (Tracit-600A, Chemax Mfg. Corp.) and then inserted a heater with a K-type thermocouple (KLCaH, Daiki Kogyo Co., Ltd.) into the hole [Fig. 2(b)]. The heater was thermally well connected to the Cu bobbin after the cement layer was dried. The high thermal conductivity of the Cu bobbin allows the efficient heat transfer from the heater to the multilayer laminate. To measure ANE in the multilayer-laminated coiled Ni-based alloy wire, the coil with the heater and thermocouple was clamped between the pole pieces of an electromagnet, and an external magnetic field was applied in the axial direction of the coil [Fig. 2(d)]. Here, to minimize heat leakage from the coil to the pole pieces, silicone rubber sheets with low thermal conductivity were inserted between them. The electric voltage between the ends of the Ni-based alloy wire was measured while heating the center of the coil at room temperature and atmospheric pressure.

Figure 3(a) shows the magnetic field H dependence of the voltage V between the ends of the Ni-based alloy wires with $N = 1$, 5, and 10 at $\Delta T = 40$ and 20 K, where ΔT is the temperature increase from room temperature at the center of the coils, measured with the thermocouples. The clear V signals were observed to appear in all the coils when finite H and ΔT were applied. The magnitude of the V signals was almost proportional to ΔT and thus the temperature gradient in the radial direction in the coils. The sign of the signals was reversed by reversing H without a field-independent offset due to the Seebeck effect. The V signals saturated for $\mu_0|H| > 150$ mT. These behaviors are consistent with the feature of ANE [Eq. (2) and Fig. 1]. Hereafter, we discuss the pure ANE voltage signals through $V_{\mathrm{ANE}} = (V_+ - V_-)/2$, where V_+ (V_-) is V at $\mu_0 H = 250$ mT (-250 mT).

In Fig. 3(b), we show V_{ANE} for the multilayer-laminated coiled Ni-based alloy wires as a function of N at $\Delta T = 40$ and 20 K. We observed the significant V_{ANE} enhancement in proportion to N. The V_{ANE} enhancement is due to the increase of the total length of the Ni-based alloy wires and the linear relationship between V_{ANE} and N confirms that the heat flux and temperature gradients are nearly constant in each layer of the multilayer laminate. However, the internal resistance R of the multilayer-laminated coiled Ni-based alloy wires also increases in proportion to N [inset of Fig. 3(c)]. As a consequence of these behaviors, the extractable output power, $V_{\mathrm{ANE}}^2/(4R)$, for the multilayer-laminated coiled Ni-based alloy wires is proportional to N [Fig. 3(c)].

The output power observed here is on the order of sub-nW, which is too small to be used in practical applications. However, there is a plenty of scope for the performance improvement. The small output power in our device is mainly due to (1) small S_{ANE} of the Ni-based alloy, (2) tiny temperature gradients in the Ni-based alloy wires because of the fact that the thermal conductivity of the alloy is much larger than that of the electrical insulation layers (i.e., PET and varnish), (3) further reduction of the temperature gradients due to the absence of heat baths or heat sinks on the outer surfaces of the coils, and (4) low winding density of the wires (partially due to the thick insulation

layers). If a magnetic wire with 10 times larger S_{ANE} is used and a temperature gradient in the magnetic wire is improved by 10 times through an optimal thermal design, the output power will be on the order of μW even with the same wire length and N. For improved thermal design, electrical insulation layers with high thermal conductivity and good thermal contact with metallic wires are necessary and the thickness of the insulation layers should be as thin as possible. By increasing N and wire density in addition to these improvements, thermal energy harvesting with sub-mW- or mW-order output power would be possible in coils with similar size (note that the output is scalable with respect to the coil length or size). To decrease the internal resistance of the thermoelectric generators and increase the optimum current density, the use of thicker magnetic wires would also be effective. Our proof-of-concept demonstration will thus provide a useful piece of information for designing ANE-based energy harvesting devices.

In conclusion, thermoelectric generation using ANE was demonstrated in the multilayer-laminated coils consisting of radially stacked ferromagnetic metal wires. When the center of the coils was heated, the thermoelectric voltage and resultant power due to ANE were found to appear and increase in proportion to the number of the stacked layers. Although this experiment was performed with heating the center of the coils, they work as thermoelectric generators even when the center is cooled, where the temperature gradient in the radial direction is reversed; the multilayer-laminated coiled magnetic wires are applicable to any pipe-shaped heat sources. This device structure will lead to the improvement of the thermoelectric performance and versatility of ANE devices.

Acknowledgments

The authors thank T. Hirai and M. Isomura for technical supports. This work was supported by CREST "Creation of Innovative Core Technologies for Nano-enabled Thermal Management" (JPMJCR17I1) and ERATO "Magnetic Thermal Management Materials" (JPMJER2201) from Japan Science and Technology Agency.

1) W.-L. Lee, S. Watauchi, V. L. Miller, R. J. Cava, and N. P. Ong, Phys. Rev. Lett. **93**, 226601 (2004).
2) T. Miyasato, N. Abe, T. Fujii, A. Asamitsu, S. Onoda, Y. Onose, N. Nagaosa, and Y. Tokura, Phys. Rev. Lett. **99**, 086602 (2007).
3) Y. Pu, D. Chiba, F. Matsukura, H. Ohno, and J. Shi, Phys. Rev. Lett. **101**, 117208 (2008).
4) M. Mizuguchi, S. Ohata, K. Uchida, E. Saitoh, and K. Takanashi, Appl. Phys. Express **5**, 093002 (2012).
5) Y. Sakuraba, K. Hasegawa, M. Mizuguchi, T. Kubota, S. Mizukami, T. Miyazaki, and K. Takanashi, Appl. Phys. Express **6**, 033003 (2013).

6) K. Uchida, T. Kikkawa, T. Seki, T. Oyake, J. Shiomi, Z. Qiu, K. Takanashi, and E. Saitoh, Phys. Rev. B **92**, 094414 (2015).
7) Y. Sakuraba, Scr. Mater. **111**, 29 (2016).
8) C. Fang, C. H. Wan, Z. H. Yuan, L. Huang, X. Zhang, H. Wu, Q. T. Zhang, and X. F. Han, Phys. Rev. B **93**, 054420 (2016).
9) M. Ikhlas, T. Tomita, T. Koretsune, M. Suzuki, D. Nishio-Hamane, R. Arita, Y. Otani, and S. Nakatsuji, Nat. Phys. **13**, 1085 (2017).
10) X. Li, L. Xu, L. Ding, J. Wang, M. Shen, X. Lu, Z. Zhu, and K. Behnia, Phys. Rev. Lett. **119**, 056601 (2017).
11) Z. Yang, E. A. Codecido, J. Marquez, Y. Zheng, J. P. Heremans, and R. C. Myers, AIP Adv. **7**, 095017 (2017).
12) A. Sakai, Y. P. Mizuta, A. A. Nugroho, R. Sihombing, T. Koretsune, M.-T. Suzuki, N. Takemori, R. Ishii, D. Nishio-Hamane, R. Arita, P. Goswami, and S. Nakatsuji, Nat. Phys. **14**, 1119 (2018).
13) S. N. Guin, K. Manna, J. Noky, S. J. Watzman, C. Fu, N. Kumar, W. Schnelle, C. Shekhar, Y. Sun, J. Gooth, and C. Felser, NPG Asia Mater. **11**, 16 (2019).
14) H. Nakayama, K. Masuda, J. Wang, A. Miura, K. Uchida, M. Murata, and Y. Sakuraba, Phys. Rev. Mater. **3**, 114412 (2019).
15) W. Zhou and Y. Sakuraba, Appl. Phys. Express **13**, 043001 (2020).
16) Y. Sakuraba, K. Hyodo, A. Sakuma, and S. Mitani, Phys. Rev. B **101**, 134407 (2020).
17) A. Sakai, S. Minami, T. Koretsune, T. Chen, T. Higo, Y. Wang, T. Nomoto, M. Hirayama, S. Miwa, D. Nishio-Hamane, F. Ishii, R. Arita, and S. Nakatsuji, Nature **581**, 53 (2020).
18) T. Seki, Y. Sakuraba, K. Masuda, A. Miura, M. Tsujikawa, K. Uchida, T. Kubota, Y. Miura, M. Shirai, and K. Takanashi, Phys. Rev. B **103**, L020402 (2021).
19) K. Uchida, W. Zhou, and Y. Sakuraba, Appl. Phys. Lett. **118**, 140504 (2021).
20) Y. Pan, C. Le, B. He, S. J. Watzman, M. Yao, J. Gooth, J. P. Heremans, Y. Sun, and C. Felser, Nat. Mater. **21**, 203 (2022).
21) K. Uchida and J. P. Heremans, Joule **6**, 2240 (2022).
22) H. Tanaka, T. Higo, R. Uesugi, K. Yamagata, Y. Nakanishi, H. Machinaga, and S. Nakatsuji, Adv. Mater., 2303416 (2023).
23) W. Zhou, K. Yamamoto, A. Miura, R. Iguchi, Y. Miura, K. Uchida, and Y. Sakuraba, Nat. Mater. **20**, 463 (2021).
24) A. Miura, H. Sepehri-Amin, K. Masuda, H. Tsuchiura, Y. Miura, R. Iguchi, Y. Sakuraba, J. Shiomi, K. Hono, and K. Uchida, Appl. Phys. Lett. **115**, 222403 (2019).

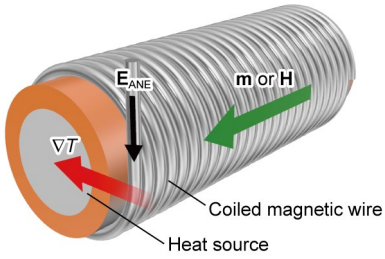

Fig. 1. Schematic of ANE in a coiled magnetic wire. $\mathbf{E}_{\mathrm{ANE}}$, **m**, **H**, and ∇T denote the electric field driven by ANE, unit vector of magnetization of the magnetic wire, direction of an external magnetic field, and temperature gradient, respectively.

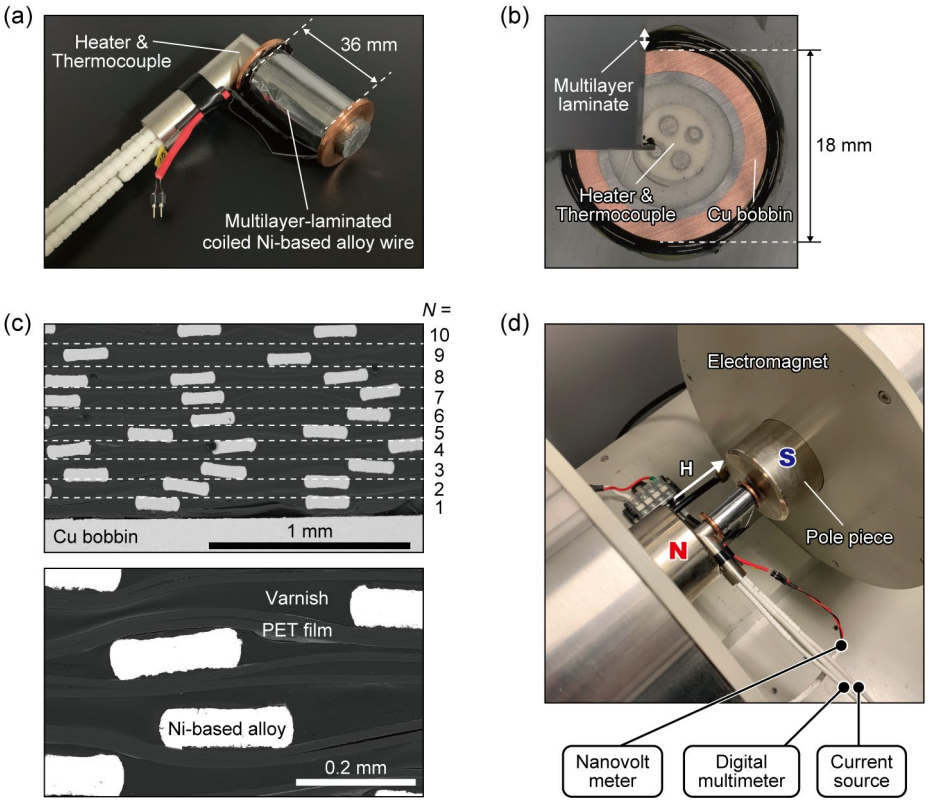

Fig. 2. (a) Photograph of the ANE-based thermoelectric generator comprising multilayer-laminated coiled Ni-based alloy wires. (b) Cross-sectional photograph of the thermoelectric generator. At the center of the Cu bobbin, the heater and thermocouple are embedded. (c) Scanning electron microscope images of the cross-section of the multilayer laminate. *N* denotes the number of the stacked layers, where each layer consists of the Ni-based alloy wires, PET films, and varnish. (d) Experimental setup for measuring ANE in the multilayer-laminated coiled Ni-based alloy wires.

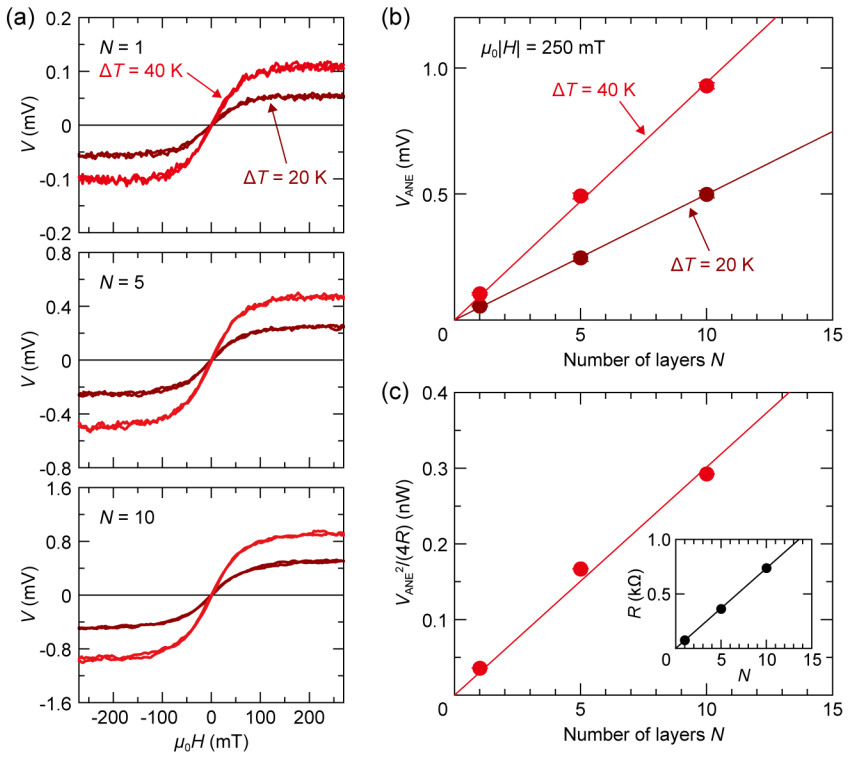

Fig. 3. (a) Magnetic field H dependence of the open-circuit voltage V in the multilayer-laminated coiled Ni-based alloy wires with $N = 1$, 5, and 10 at $\Delta T = 40$ and 20 K. ΔT denotes the temperature increase from room temperature at the center of the coil. (b) N dependence of the ANE voltage V_{ANE} at $\Delta T = 40$ and 20 K and $\mu_0|H| = 250$ mT. (c) N dependence of the extractable power $V_{\mathrm{ANE}}^2/(4R)$ at $\Delta T = 40$ K and $\mu_0|H| = 250$ mT. The inset shows the N dependence of the resistance R between the ends of the Ni-based alloy wires. μ_0 is the vacuum permeability.